Flame transfer function measurement of a sequential combustor fuelled with natural gas and hydrogen

Author(s):
Dharmaputra, Bayu; Nagpure, Pushkin; Impagnatiello, Matteo; Noiray, Nicolas

Publication date:
2025-04

Permanent link:
https://doi.org/https://doi.org/10.3929/ethz-b-000717430

Originally published in:
Combustion and Flame 274, https://doi.org/10.1016/j.combustflame.2025.113972

Funding acknowledgement:
- ThermoacOustic instabilities contRol in sequential Combustion cHambers ()

Combustion and Flame 274 (2025) 113972

Contents lists available at ScienceDirect

Combustion and Flame

journal homepage: www.sciencedirect.com/journal/combustion-and-flame

Brief Communication

Flame transfer function measurement of a sequential combustor fuelled with natural gas and hydrogen

Bayu Dharmaputra *, Pushkin Nagpure, Matteo Impagnatiello, Nicolas Noiray *

CAPS Laboratory, Department of Mechanical and Process Engineering, ETH Zürich, 8092, Zürich, Switzerland

ARTICLE INFO

Keywords:
Flame transfer function
Sequential combustor
Thermoacoustic instabilities

ABSTRACT

The flame transfer function (FTF) relates acoustic perturbations and the coherent heat release rate response. This frequency-dependent function governs the thermoacoustic stability of a combustor. The FTF measurement is therefore of great interest for predicting the stability of the practical combustor connected to the engine's compressor and turbine. So far, the FTFs of the second stage of constant pressure sequential combustors (CPSC) have only been obtained from numerical simulations. In this study, second-stage FTFs are measured experimentally. The thermal power of the first- and second-stage flames is configured to be equal. The effects of hydrogen blending in the first- and second-stage fuel mixtures on the sequential FTF are analyzed. The FTF of the sequential flame is fitted with a distributed time delay (DTD) model with two pulses. The trends of the model parameters obtained are consistent with the OH^* chemiluminescence of the sequential flame.

Novelty and significance

In this study, the flame transfer function of the second-stage flame of an atmospheric sequential combustor is measured for the first time. This is a significant progress as the second stage FTF has been obtained so far only from numerical simulations. The effects of the amount of hydrogen mixture in the first- and second-stage fuels on the sequential flame transfer function are investigated. This work thus serves as a stepping stone toward the thermoacoustic modeling of a sequential combustor for stability predictions.

1. Introduction

Modern gas turbines for electric power production must achieve fast ramp-up and ramp-down times to balance the inherent intermittency of wind and solar power sources. The constant pressure sequential combustor (CPSC) is a promising solution to these challenges [1]. The CPSC offers numerous advantages, including high fuel flexibility, ability to burn a significant amount of hydrogen, a wide load operational range, and low NOx and CO emissions over a wide operating range [2,3].

However, as in single-stage combustor architectures, the operational range of CPSCs is limited by thermoacoustic instabilities. One of the key information that needs to be quantified to predict these thermoacoustic instabilities is the flame transfer function (FTF). The FTF relates the heat release rate fluctuations of the flame to the upstream velocity perturbations. The FTFs of single-stage combustors have been widely studied in both laboratory-scale setups, e.g. [4–8] and industrial setups [9,10].

To the best of our knowledge, the FTF of CPSC's second stages have only been characterized by numerical simulations [11–14] and analytical methods [15,16], and no experimental FTFs have been measured so far.

In this study, we aim at filling this knowledge gap by experimentally measuring the second-stage FTF of an atmospheric sequential combustor. In particular, we investigate the effect of hydrogen blending in both first- and second-stage fuel lines on the FTF. Furthermore, we fit the measured FTFs using the widely known distributed time delay (DTD) model [17], and show that for the forcing amplitudes considered here, the response of the reheat flame to acoustic excitation exhibits the characteristics of a technically premixed first-stage flame with stiff fuel injection.

2. Experimental setup

The sequential combustor setup, similar to that in [18,19], is briefly described here. Figure 1 shows the side view of the setup for FTF measurements. It includes a plenum with loudspeakers (Beyma model CP-755Nd) for acoustic forcing, a fully premixed matrix burner composed of 4 × 4 channels of ø6 mm, a combustion chamber with a 62×62 mm^2 cross-section, and a sequential burner with a mixing channel (25×38 mm^2 cross-section). Secondary fuel is injected 178 mm

* Corresponding authors.
E-mail addresses: bayud@ethz.ch (B. Dharmaputra), noirayn@ethz.ch (N. Noiray).

https://doi.org/10.1016/j.combustflame.2025.113972
Received 6 August 2024; Received in revised form 6 January 2025; Accepted 7 January 2025
Available online 21 January 2025

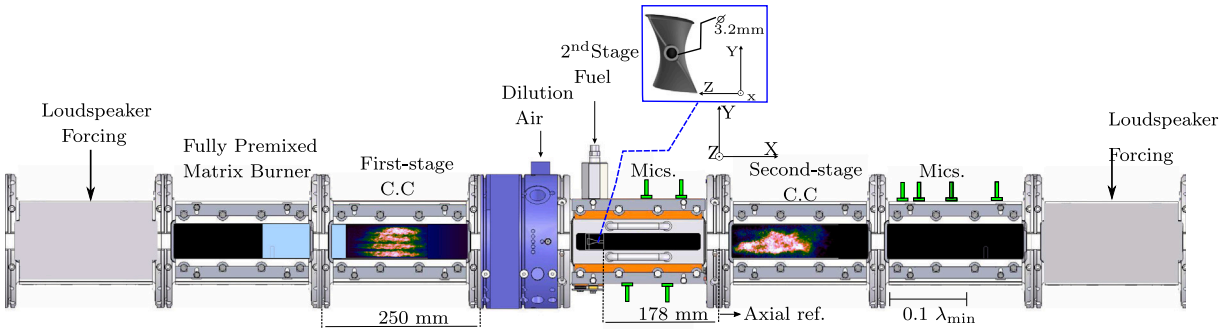

Fig. 1. Experimental setup for sequential flame transfer function investigations. C.C: combustion chamber, Mics.: Microphones, $\lambda_{\min} = c_{ds}/f_{\max}$ (minimum acoustic wavelength downstream of the flame). The inset shows the X-lobe fuel injector.

from the burner outlet, through an X-lobe injector of ⌀3.2 mm to introduce a rotational movement for enhancing the mixing between the vitiated flow and the fuel. A second pair of loudspeakers is located downstream of the second-stage combustion chamber. Both sets of loudspeakers provide an acoustic forcing from 190 Hz to 700 Hz with a step of 10 Hz. First-stage air with a mass-flow of 17 g/s is preheated to 250 °C, and a hydrogen-natural gas blend is injected upstream of the loudspeakers, creating a premixed mixture. Dilution air with a mass flow of 18 g/s is injected downstream of the first-stage combustion chamber.

The tunable diode laser absorption spectroscopy with wavelength modulation spectroscopy (TDLAS-WMS) method, which can measure relatively low coherent temperature fluctuations down to 5 K as detailed in [20] and verified with numerical simulations in [21,22], measures the line of sight integrated temperature at 10 cm downstream of the second-stage fuel injection in the mixing channel, aligned similarly to the setup in [23]. However, no coherent temperature fluctuations are detected in the acoustic frequency band of interest for the acoustic forcing amplitudes considered. Additionally, the expected isentropic relative temperature fluctuations induced by the pressure perturbations is about 0.06% which equals to 0.72 K. This level of temperature fluctuation cannot be resolved with the TDLAS-WMS method.

Four flush-mounted G.R.A.S microphones are placed along the sequential mixing channel walls, with another four downstream of the second-stage combustion chamber. Both sets of microphones are used to reconstruct the acoustic variables upstream and downstream of the reference location, which in this case is the sequential burner outlet, with the multi-microphone method (MMM) [24]. A high-speed intensified camera (LaVison Star X + LaVision HS-IRO) equipped with a CERCO UV lens (45 mm, F/1.8 Cerco) and a bandpass filter (Edmund Optics, centered at 310 nm, FWHM 10 nm) is pointed at the sequential flame to capture the OH^* chemiluminescence.

The hydrogen blending mass fractions for the first and second stage fuel, denoted by $Y_{H_2}^{1st}$ and $Y_{H_2}^{2nd}$, are defined as the ratio of hydrogen mass flow to the total mass flow of hydrogen and natural gas in each fuel line. In this study, both quantities are varied, but the total thermal power of both flames is kept constant at 77 kW and in a 1:1 ratio for all operating conditions. Both flames are in lean condition, with equivalence ratio ranges of 0.74–0.77 and 0.54–0.6 for the first flame and sequential flame, respectively. The flow velocity inside the mixing channel remains around 110 m/s, with a temperature of about 1200 K for all cases. It is worth mentioning that for all operating conditions, no ignition kernel is generated inside the mixing channel.

3. Methodology

For the remainder of the manuscript, the subscripts $(.)_{us}$ and $(.)_{ds}$ represent the quantities upstream and downstream of the flame, respectively. The relative heat release rate fluctuations, $\dot{Q}'/\overline{\dot{Q}}$, can be written as a function of the relative upstream pressure $(p'_{us}/\overline{p}_{us})$, velocity $(u'_{us}/\overline{u}_{us})$, equivalence ratio $(\phi'/\overline{\phi})$, and temperature fluctuations $(T'_{us}/\overline{T}_{us})$ as discussed in [12,14,25]. We adopt here the description used in [25]:

$$\frac{\dot{Q}'}{\overline{\dot{Q}}} = F_p \frac{p'_{us}}{\overline{p}_{us}} + F_u \frac{u'_{us}}{\overline{u}_{us}} + F_T \frac{T'_{us}}{\overline{T}_{us}}. \tag{1}$$

The expression above does not explicitly account for equivalence ratio fluctuations, whose effects are embedded in the other transfer functions, as will be shown later.

As mentioned previously, the TDLAS-WMS does not detect coherent temperature fluctuations, T'_{us}, in the frequency and forcing amplitude ranges of interest. Therefore, in this study, F_T is not quantified and we could resort to the classical 2 × 2 flame transfer matrix (FTM) identification approach as described in [4,6]. From the Rankine Hugoniot relationships, the acoustic velocity fluctuations downstream of the sequential flame (u'_{ds}) can be written as a function of the F_{21} and F_{22} elements of the flame transfer matrix (FTM):

$$\begin{aligned} u'_{ds} &= F_{21}\frac{p'_{us}}{(\bar{\rho}\bar{c})_{us}} + F_{22}u'_{us} \\ &= \gamma\theta M_{us}(F_p - 1)\frac{p'_{us}}{(\bar{\rho}\bar{c})_{us}} + (1 + \theta F_u)u'_{us} \\ \theta &= \frac{\overline{T}_{ds}}{\overline{T}_{us}} - 1, \end{aligned} \tag{2}$$

where γ and M_{us} are the ratio of the specific heat capacities and the upstream Mach number, respectively.

The F_{21} element of the FTM that we measured exhibits a very low gain of about 5% of $|F_{22}|$ in the frequency range of interest for all operating conditions. Hence, in this study, we focus only on the F_{22} element. It is worth mentioning that in our measurements, the relative upstream velocity perturbations, $u'_{us}/\overline{u}_{us}$, range around 1%–3% for the frequency ranges and all the operating conditions considered. The F_u in Eq. (2) is the classical FTF and can be obtained from F_{22}: $F_u = (F_{22} - 1)/\theta$. The obtained FTF is then fitted to a DTD model, described in [17], with two Gaussian pulses:

$$\mathrm{FTF}(\omega) = n_1 \exp\left(-i\omega\tau_1 - \frac{\omega^2\sigma_1^2}{2}\right) + n_2 \exp\left(-i\omega\tau_2 - \frac{\omega^2\sigma_2^2}{2}\right), \tag{3}$$

where τ_k and σ_k model the time delay and the characteristic spread of each pulse, respectively. By looking again at the experimental setup in Fig. 1, one can see that the sequential flame configuration is close to a technically premixed configuration. This implies that the upstream acoustic perturbations will additionally generate equivalence ratio perturbations ϕ'. Therefore, the FTF gain at 0 Hz must be equal to zero [26]. An example of FTF obtained through numerical simulation that is similar to our configuration could be seen in [11], where the FTF gain goes to 0 at 0 Hz, and the phase approaches $\pi/2$. In order to fulfill this criterion, a constraint is added to the FTF model:

$$n_1 + n_2 = 0, \text{and } n_1 \equiv n. \tag{4}$$

The first time delay pulse models the perturbations generated at the dump plane of the sequential burner which are induced by the acoustic perturbations and advected by the mean flow. The second time

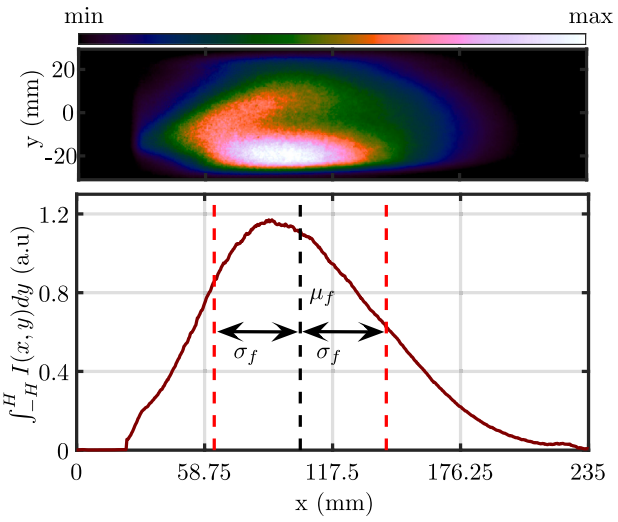

Fig. 2. (top) Averaged OH*chemiluminescence at $Y_{H_2}^{2nd}$ = 7.4% and $Y_{H_2}^{1st}$ = 4.8%. (bottom) The vertically integrated OH*chemiluminescence intensity, with the flame center of mass, μ_f, indicated by the black dashed line. The flame characteristic width, σ_f, is represented by the distance between the black dashed line and the red dashed lines. (For interpretation of the references to color in this figure legend, the reader is referred to the web version of this article.)

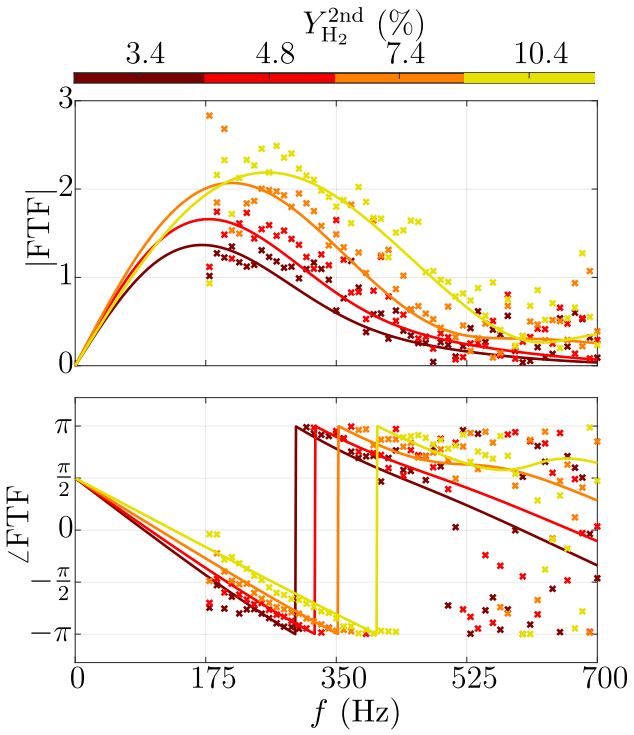

Fig. 3. Measured (symbols) and fitted FTFs (solid lines) for different $Y_{H_2}^{2nd}$. The $Y_{H_2}^{1st}$ is fixed at 4.8%. Two DTDs are employed for the fitting according to Eqs. (3) and (4). The gain and phase of FTFs are shown on the top and bottom plot, respectively.

delay models the convected equivalence ratio perturbations that are generated at the sequential fuel injector. This rationale for modeling is similar to the FTF model for technically premixed matrix flames described in [6]. Hence, one can expect that the difference between τ_2 and τ_1 is equal to the fuel residence time in the mixing channel. The validity of this assumption will be verified in the next section.

To characterize the flame length and spread, the 2D image of the OH* chemiluminescence, $I(x, y)$, is integrated along the vertical axis (Y-axis in Fig. 1): $I(x) = \int_{-H/2}^{H/2} I(x, y)dy$. The center of mass of the flame, μ_f, and the characteristic width, σ_f, are then computed as:

$$\mu_f = \frac{\int xI(x)dx}{\int I(x)dx} \tag{5}$$

$$\sigma_f^2 = \frac{\int (x-\mu_f)^2 I(x)dx}{\int I(x)dx}. \tag{6}$$

The time-averaged OH* intensity is utilized as a qualitative marker to identify flame characteristics, acknowledging that its fluctuations do not directly represent heat release rate variations. This approach is supported by prior studies that demonstrated a strong correlation between time-averaged OH* chemiluminescence and the averaged flame heat release rate in similar configurations [27,28]. Figure 2 shows the averaged OH*chemiluminescence at $Y_{H_2}^{2nd}$ = 7.4% and $Y_{H_2}^{1st}$ = 4.8%. The chemiluminescence image is vertically integrated to derive the axial distribution of OH*, which is then used to compute μ_f and σ_f, as illustrated in the bottom plot of Fig. 2. Zero-dimensional (0D) simulations are performed using Cantera to compute the expected ignition delays of the sequential mixtures, as outlined in the supplementary material. For all operating conditions, the expected ignition delay is significantly larger than the sequential fuel residence time and the high-speed camera does not detect any ignition kernels in the mixing channel.

4. Results and discussion

4.1. Variations of hydrogen blending in the sequential fuel line

The measured FTFs and their corresponding best fit with Eq. (3) for different $Y_{H_2}^{2nd}$ are shown in Fig. 3. Note that in these cases, the $Y_{H_2}^{1st}$ is fixed at 4.8%. As can be seen, the gain of FTF exhibits noticeable variations with respect to the variations in $Y_{H_2}^{2nd}$. Furthermore, the slope of the phase becomes flatter as $Y_{H_2}^{2nd}$ increases. This indicates that there is a decrease in the characteristic time delay of the perturbations, which can be related to the change in the shape of the sequential flame as will be discussed below.

Figure 4a shows the DTD parameters of the FTF fitting. It is important to note that, for the FTF fitting, only the data between 210 Hz and 600 Hz are utilized. Outside this range, the FTF gain and phase have relatively large uncertainties for all operating conditions, as shown in the supplementary material. Figure 4b shows the vertically integrated flame chemiluminescence at different hydrogen fractions in the sequential fuel line. As can be seen, the flame moves closer to the burner outlet as $Y_{H_2}^{2nd}$ increases. This behavior is expected as the fuel reactivity also increases. Both the μ_f and σ_f exhibit monotonically decreasing trends with respect to $Y_{H_2}^{2nd}$. The trends of σ and τ from the fitting of the model are consistent with those of the flame chemiluminescence as shown in Fig. 4a and 4b. Furthermore, the identified time delays (τ_1, τ_2) are significantly smaller than the expected ignition delay under all operating conditions.

Indeed, the mean time delay parameters τ_1 and τ_2 decrease with increasing hydrogen fraction in the sequential fuel line, attributed to flame shortening as shown in Fig. 4b. The difference between the time delays, $\Delta\tau = \tau_2 - \tau_1$, remains constant at approximately 1.6 ms across different hydrogen blending amounts. This matches the expected convective delay, $\tau_{conv} = L/\overline{U}_{conv} = 0.178/110 \approx 1.6$ ms, given the flow velocity of 110 m/s and the 178 mm distance between the sequential fuel injector and the dump plane. It is important to note that this study does not aim to quantitatively correlate σ_f and μ_f with τ_k and σ_k, as such an analysis would necessitate additional velocimetry measurements. Instead, the key observation is that (τ_k, σ_k) and (μ_f, σ_f) demonstrate similar trends with variations in hydrogen blending.

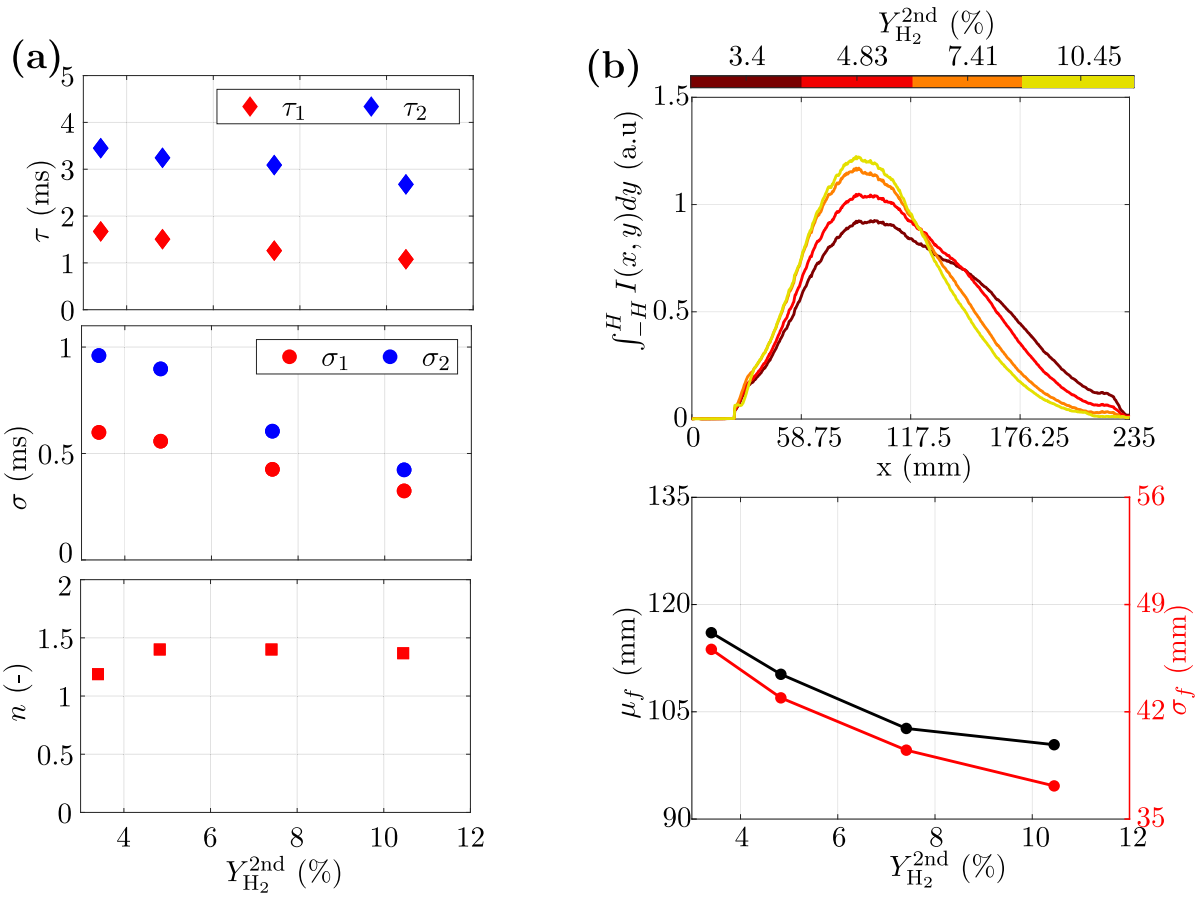

Fig. 4. (a) The resulting mean time delay τ, time delay spread σ and gain n parameters from the fitting of the flame transfer function across different hydrogen blending in the second-stage fuel line, $Y^{2nd}_{H_2}$. (b) The vertically integrated flame chemiluminescence at different $Y^{2nd}_{H_2}$ (top) along with the flame center of mass and characteristic width (bottom).

4.2. Variations of hydrogen blending in the first stage fuel line.

In the second test case, $Y^{2nd}_{H_2}$ is fixed at 10.45%, and $Y^{1st}_{H_2}$ is varied from 1.3 to 7.4%. Note that the thermal power of the first-stage flame is kept constant, therefore the temperature in the mixing channel is only weakly affected. The measured FTFs and the resulting model fittings can be seen in Fig. 5. In contrast to the previous case, both the gain and phase of the FTFs show no significant variation with respect to changes in $Y^{1st}_{H_2}$.

The vertically integrated flame chemiluminescence for this test case is shown in Fig. 6b and it can be seen that the shape does not change significantly between different $Y^{1st}_{H_2}$. Furthermore, the flame center of mass and characteristic width show no clear trend. This observation is aligned again with the resulting DTD parameters from the FTF fittings. The mean time delay τ remains constant and its spread σ does not vary as significantly as in the previous case where $Y^{2nd}_{H_2}$ is varied. The concentrations of major species in the mixing channel after dilution air injection remain nearly identical across different $Y^{1st}_{H_2}$ values, as shown in the supplementary material. Additionally, the constant thermal power of the first stage ensures a stable temperature of approximately 1200 K. This consistency aligns with the observed similarity in the FTFs and the overall flame shape.

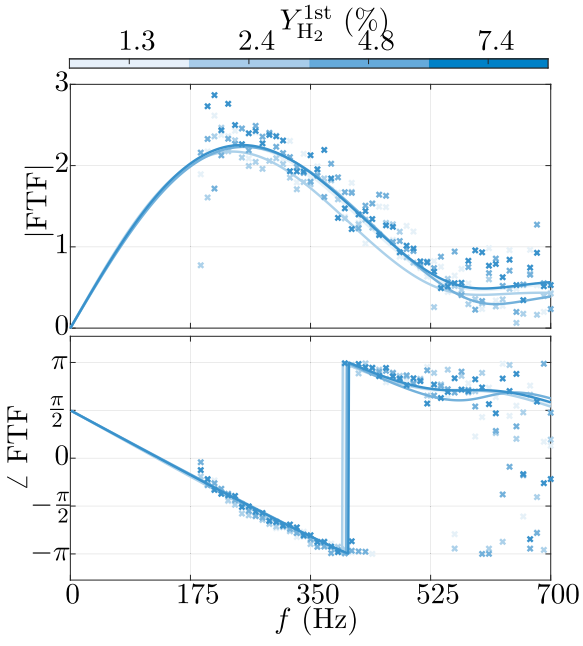

Fig. 5. Measured (symbols) and fitted FTFs (solid lines) at different $Y^{1st}_{H_2}$. $Y^{2nd}_{H_2}$ is fixed at 10.45%. Two DTDs are employed for the fitting. The gain and phase of FTFs are shown on the top and bottom plot, respectively.

5. Conclusions and outlook

This study experimentally quantifies the sequential flame transfer function (FTF) of an atmospheric sequential combustor. The results reveal that the sequential FTF is sensitive to hydrogen blending in the second-stage fuel line but remains largely unaffected by hydrogen

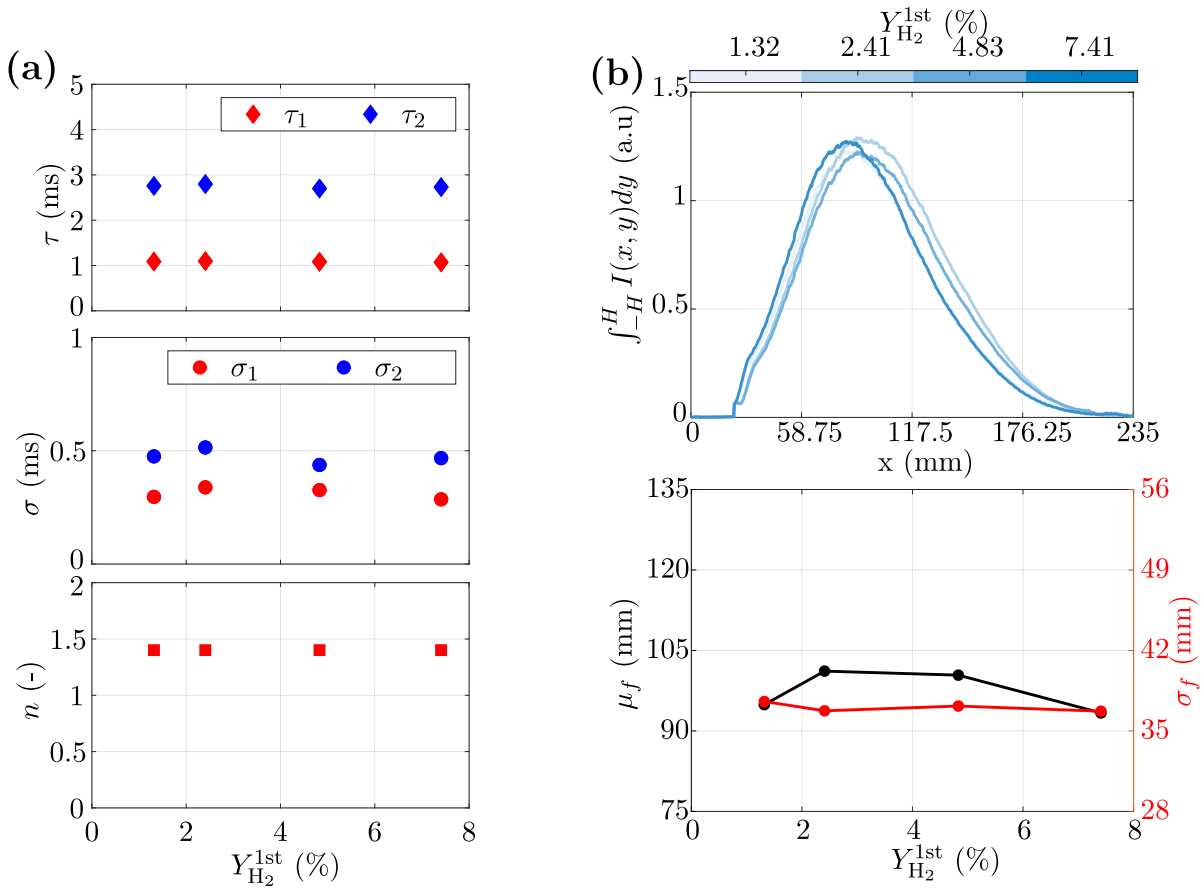

Fig. 6. (a) The resulting mean time-delay τ, time delay spread σ and gain n parameters from the fitting of the flame transfer function across different hydrogen blending in the first-stage fuel line, $Y_{H_2}^{1st}$. (b) The vertically integrated flame chemiluminescence at different $Y_{H_2}^{1st}$ (top) along with the flame center of mass and characteristic width (bottom).

blending in the first-stage fuel line. By employing the classical distributed time delay (DTD) model, the sequential FTF can be effectively fitted with two distinct pulses. Higher hydrogen blending in the second-stage fuel mixture results in a more compact and shorter sequential flame. The observed trends in the mean time delay parameters (τ_1, τ_2) and the characteristic spread parameters (σ_1, σ_2) are in close agreement with the observed changes in the flame center of mass and characteristic width.

This first measurement of CPSC's second-stage FTF paves the way for future studies, such as the FTF measurement of the first-stage flame for stability analyses of the whole thermoacoustic system or the measurement of the second-stage flame describing function (FDF) by forcing it at larger amplitude. Furthermore, by employing the same methodology, the effects of nanosecond repetitively pulsed discharges (NRPD) on the sequential FTF can be quantified. This would then provide a quantitative explanation on the stabilizing effect of NRPD on the thermoacoustic of a sequential combustor, which was demonstrated in [18].

Authorship contribution statement

B.D. and **N.N.** conceived the research idea. **B.D.** led the experimental investigations. **B.D.**, **P.N.** and **M.I.** performed the experiments. **B.D.** and **P.N.** analyzed the data. **B.D.**, **P.N.**, **M.I.** and **N.N.** discussed the results. **B.D.** drafted the manuscript with the support of **N.N.** The final version of the manuscript has been edited and approved by **B.D.**, **P.N.**, **M.I.** and **N.N.**

Declaration of competing interest

The authors declare that they have no known competing financial interests or personal relationships that could have appeared to influence the work reported in this paper.

Acknowledgment

This project has received funding from the European Research Council (ERC) under the European Union's Horizon 2020 research and innovation program (grant agreement No [820091]).

Appendix A. Supplementary data

Supplementary material related to this article can be found online at https://doi.org/10.1016/j.combustflame.2025.113972.

References

[1] D.A. Pennell, M.R. Bothien, A. Ciani, V. Granet, G. Singla, S. Thorpe, A. Wickstroem, K. Oumejjoud, M. Yaquinto, An introduction to the ansaldo GT36 constant pressure sequential combustor, Proc. ASME Turbo Expo 4B (2017).
[2] A. Ciani, M. Bothien, B. Bunkute, J. Wood, G. Früchtel, Superior fuel and operational flexibility of sequential combustion in Ansaldo Energia gas turbines, J. Glob. Power Propuls. Soc. 3 (2019) 630–638.
[3] M.R. Bothien, A. Ciani, J.P. Wood, G. Fruechtel, Sequential combustion in gas turbines: the key technology for burning high hydrogen contents with low emissions, in: Turbo Expo: Power for Land, Sea, and Air, vol. 4A: Combustion, Fuels, and Emissions, 2019.

[4] A. Blondé, B. Schuermans, K. Pandey, N. Noiray, Effect of hydrogen enrichment on transfer matrices of fully and technically premixed swirled flames, J. Eng. Gas Turbines Power 145 (2023) 121009.
[5] F. Di Sabatino, T.F. Guiberti, W.R. Boyette, W.L. Roberts, J.P. Moeck, D.A. Lacoste, Effect of pressure on the transfer functions of premixed methane and propane swirl flames, Combust. Flame 193 (2018) 272–282.
[6] K. Moon, R. Martin, B. Schuermans, N. Noiray, Transfer functions of lean fully- and technically-premixed jet-stabilized turbulent hydrogen flames, Proc. Combust. Inst. 40 (2024) 105256.
[7] P.M. zur Nedden, M.E.G. Eck, F. Lückoff, L. Panek, A. Orchini, C.O. Paschereit, Flame transfer function and emissions of a piloted single jet burner: influence of hydrogen content, in: Turbo Expo: Power for Land, Sea, and Air, vol. 3B: Combustion, Fuels, and Emissions, 2023, V03BT04A017.
[8] E. Æsøy, H.T. Nygård, N.A. Worth, J.R. Dawson, Tailoring the gain and phase of the flame transfer function through targeted convective-acoustic interference, Combust. Flame 236 (2022) 111813.
[9] B. Schuermans, F. Guethe, W. Mohr, Optical transfer function measurements for technically premixed flames, J. Eng. Gas Turbines Power 132 (2010) 081501.
[10] T. John, N. Magina, F. Han, J. Kaufmann, M. Vogel, T. Sattelmayer, Modeling flame transfer functions of an industrial premixed burner, J. Eng. Gas. Turbines Power 146 (2023) 051015.
[11] Y. Yang, N. Noiray, A. Scarpato, O. Schulz, K.M. Düsing, M. Bothien, Numerical analysis of the dynamic flame response in alstom reheat combustion systems, in: Turbo Expo: Power for Land, Sea, and Air, vol. 4A: Combustion, Fuels and Emissions, 2015, V04AT04A048.
[12] F. Gant, A. Cuquel, M.R. Bothien, Autoignition flame transfer matrix: Analytical model versus large eddy simulations, Int. J. Spray Combust. Dyn. 14 (2022) 72–81.
[13] M. Impagnatiello, Q. Malé, N. Noiray, Acoustic scattering of a sequential combustor controlled with non-equilibrium plasma: A numerical study, Proc. Combust. Inst. 40 (2024) 105389.
[14] O. Schulz, N. Noiray, Autoignition flame dynamics in sequential combustors, Combust. Flame 192 (2018) 86–100.
[15] H.S. Gopalakrishnan, A. Gruber, J.P. Moeck, Computation and prediction of intrinsic thermoacoustic oscillations associated with autoignition fronts, Combust. Flame 254 (2023) 112844.
[16] F. Gant, B. Bunkute, M.R. Bothien, Reheat flames response to entropy waves, Proc. Combust. Inst. 38 (2021) 6271–6278.
[17] W. Polifke, Modeling and analysis of premixed flame dynamics by means of distributed time delays, Prog. Energ. Combust. Sci. 79 (2020) 100845.
[18] B. Dharmaputra, S. Shcherbanev, B. Schuermans, N. Noiray, Thermoacoustic stabilization of a sequential combustor with ultra-low-power nanosecond repetitively pulsed discharges, Combust. Flame 258 (2023) 113101.
[19] B. Dharmaputra, P. Reckinger, B. Schuermans, N. Noiray, BOATS: bayesian optimization for active control of thermoacoustics, J. Sound. Vib 582 (2024) 118415.
[20] B. Dharmaputra, S. Shcherbanev, A. Blondé, B. Schuermans, N. Noiray, Entropy transfer function measurement with tunable diode laser absorption spectroscopy, Proc. Combust. Inst. 39 (2023) 4621–4630.
[21] A.J. Eder, B. Dharmaputra, M. Désor, C.F. Silva, A.M. Garcia, B. Schuermans, N. Noiray, W. Polifke, Generation of entropy waves by fully premixed flames in a non-adiabatic combustor with hydrogen enrichment, J. Eng. Gas Turbines Power 145 (2023) 111001.
[22] A.J. Eder, B. Dharmaputra, A.M. Garcia, C.F. Silva, W. Polifke, Identification of entropy waves in a partially premixed combustor, Proc. Combust. Inst. 40 (2024) 105609.
[23] R. Solana-Pérez, S.A. Shcherbanev, B. Dharmaputra, A. Ciani, N. Noiray, Combustion regime transition of H2 flames during steady and transient operation of a sequential combustor, Proc. Combust. Inst (2022).
[24] C.O. Paschereit, B. Schuermans, W. Polifke, O. Mattson, Measurement of transfer matrices and source terms of premixed flames, J. Eng. Gas Turbines Power 124 (2002) 239–247.
[25] M. Bothien, D. Lauper, Y. Yang, A. Scarpato, Reconstruction and analysis of the acoustic transfer matrix of a reheat flame from large-eddy simulations, J. Eng. Gas Turbines Power 141 (2018) 021018.
[26] W. Polifke, C. Lawn, On the low-frequency limit of flame transfer functions, Combust. Flame 151 (2007) 437–451.
[27] Q. Malé, N. Barléon, S. Shcherbanev, B. Dharmaputra, N. Noiray, Numerical study of nitrogen oxides chemistry during plasma assisted combustion in a sequential combustor, Combust. Flame 260 (2024) 113206.
[28] Q. Malé, S. Shcherbanev, M. Impagnatiello, N. Noiray, Stabilization of a thermoacoustically unstable sequential combustor using non-equilibrium plasma: Large eddy simulation and experiments, Proc. Combust. Inst. 40 (2024) 105277.